

Unsupervised machine learning for time-lapse seismic studies and reservoir monitoring

Marwa Hussein¹, Robert R. Stewart², Deborah Sacrey³, David H. Johnston⁴, and Jonny Wu²

Abstract

Time-lapse (4D) seismic analysis plays a vital role in reservoir management and reservoir simulation model updates. However, 4D seismic data are subject to interference and tuning effects. Being able to resolve and monitor thin reservoirs of different quality can aid in optimizing infill drilling or in locating bypassed hydrocarbons. Using 4D seismic data from the Maui field in the offshore Taranaki Basin of New Zealand, we generate typical seismic attributes sensitive to reservoir thickness and rock properties. We find that spectral instantaneous attributes extracted from time-lapse seismic data illuminate more detailed reservoir features compared with those same attributes computed on broadband seismic data. We have developed an unsupervised machine-learning workflow that enables us to combine eight spectral instantaneous seismic attributes into single classification volumes for the baseline and monitor surveys using self-organizing maps (SOMs). Changes in the SOM natural clusters between the baseline and monitor surveys suggest production-related changes that are caused primarily by water replacing gas as the reservoir is being swept under a strong water drive. The classification volumes also facilitate monitoring water saturation changes within thin reservoirs (ranging from very good to poor quality) as well as illuminating thin baffles. Thus, these SOM classification volumes indicate internal reservoir heterogeneity that can be incorporated into reservoir simulation models. Using meaningful SOM clusters, geobodies are generated for the baseline and monitor SOM classifications. The recoverable gas reserves for those geobodies are then computed and compared with production data. The SOM classifications of the Maui 4D seismic data seem to be sensitive to water saturation change and subtle pressure depletions due to gas production under a strong water drive.

Introduction

Time-lapse seismic monitoring is an important tool in reservoir management and successful drilling planning (e.g., Calvert, 2005; Johnston, 2010). Time-lapse seismic data provide key information that is used to predict dynamic reservoir property changes (i.e., hydrocarbon saturation and/or pressure changes) because of production and to constrain reservoir simulation models through a 4D close-the-loop process (Gouveia et al., 2004; MacBeth et al., 2006; Tian et al., 2014; Nasser et al., 2017). However, because of computation limitations, flow simulation models usually have coarser grid blocks compared with geologic models (Doyen, 2007). Thus, these flow simulation models may not account for detailed reservoir heterogeneities, which

can cause mismatches between the modeled seismic response and the actual 4D seismic amplitude (Sengupta et al., 2003; Helgerud et al., 2011).

Similar to 3D seismic, 4D seismic data are subject to wavelet interference and tuning thickness effects (Johnston, 2013). Moving toward quantitative 4D interpretation and improving the seismic resolution, Bayesian-based probabilistic inversion can be used to quantify reservoir property changes and get uncertainty estimates. These inversion processes gradually perturb the reservoir property changes at each trace until the mismatch between the synthetic and actual seismic traces is minimized (Baland and El Ouair, 2006; Kleemeyer et al., 2012; Xue, 2013; Grana and Mukerji, 2015). However, this requires accurate wavelet and

¹Formerly University of Houston, Department of Earth and Atmospheric Sciences, Houston, Texas 77204, USA; presently Ain Shams University, Department of Geophysics, Cairo 11566, Egypt. E-mail: marwa.eweis@sci.asu.edu.eg (corresponding author).

²University of Houston, Department of Earth and Atmospheric Sciences, Houston, Texas 77204, USA. E-mail: rrstewar@central.uh.edu; jwu40@central.uh.edu.

³Auburn Energy, Weimar, Texas 77024, USA. E-mail: dsacrey@auburnenergy.com

⁴Differential Seismic LLC, Houston, Texas 77079, USA. E-mail: dhjohnston@sbcglobal.net.

Manuscript received by the Editor 8 August 2020; revised manuscript received 11 February 2021; published ahead of production 13 April 2021; published online 01 July 2021. This paper appears in *Interpretation*, Vol. 9, No. 3 (August 2021); p. T791–T807, 10 FIGS.

<http://dx.doi.org/10.1190/INT-2020-0176.1>. © 2021 The Authors. Published by the Society of Exploration Geophysicists and the American Association of Petroleum Geologists. All article content, except where otherwise noted (including republished material), is licensed under a Creative Commons Attribution 4.0 Unported License (CC BY). See <https://creativecommons.org/licenses/by/4.0/>. Distribution or reproduction of this work in whole or in part commercially or noncommercially requires full attribution of the original publication, including its digital object identifier (DOI).

rock-physics models, which may be challenging to achieve for complex reservoir dynamics (Cao and Roy, 2017). Bayesian inversions may not discriminate between shale and thinly bedded sand-shale sequences because of seismic resolution challenges. Although thin sands may not have a significant contribution to the volume of recoverable hydrocarbon, those sands can influence fluid flow. If they are not captured in the geologic and flow simulation models, there can be a mismatch between the model and the 4D seismic data (Nasser et al., 2017).

To understand reservoir heterogeneity and to resolve thin reservoirs, spectral decomposition attributes have been applied in various time-lapse projects for different geologic settings (Zhao et al., 2006; Rojas and Davis, 2009; White et al., 2015). Most recently, Grochau and Jilinski (2016) test spectral decomposition analysis on synthetic difference volumes generated for a presalt carbonate reservoir. They derive production facies classifications based on the spectral decomposition difference volumes using probability density functions. They show that the spectral decomposition difference volumes capture reservoir heterogeneity and that the classification volume illuminated water-saturation-increase facies that can be correlated to known reference water saturation changes. However, the clusters interpreted to be pressure-related showed a poorer correlation to the known pressure changes. Grochau and Jilinski's (2016) approach required time-lapse logging to calibrate the difference spectral decomposition and classification volumes. Unfortunately, time-lapse well data are rarely acquired (Cao and Roy, 2017).

In the absence of the time-lapse logs, an alternative approach is to gather reservoir information from multiple seismic attributes computed on the baseline and monitor volumes using an unsupervised machine-learning method, such as self-organizing maps (SOMs). An advantage of the SOM is its ability to resolve thin beds (Rodén et al., 2017). We show this approach by using 4D seismic data from the Maui field in the offshore Taranaki Basin, New Zealand. We begin this study by discussing the conventional interpretation of Maui 4D data. We then compute typical spectral and instantaneous attributes of the baseline and monitor volumes for the C1 Sand reservoir. We develop a workflow to carefully select a combination of seismic attributes that can be input to the SOM analysis that is used to integrate the preproduction and postproduction reservoir information in the baseline and monitor data into classification volumes. The clustered volumes enable an understanding of reservoir heterogeneity and illuminate water sweep by correlating SOM classes to well data, production data, and attribute volumes. The SOM classifications also enable monitoring production-related changes within thin reservoirs that contain very good to moderate-quality sand (also known as high-speed and normal reservoir flow units) and in poor-quality reservoirs, which cannot be monitored on the original 4D amplitude volumes. Geobodies are extracted from

meaningful clusters of SOM volumes (i.e., those clusters that are correlated to the well data and show changes in the SOM cluster patterns, which agree with the 4D difference volumes and production data) and are then used to calculate recoverable gas for the baseline and monitor time steps. The difference of these estimates is compared with estimates obtained from geobodies extracted from the amplitude difference and to production data. Finally, we discuss the limitations of the workflow and present some ideas on how to deal with those limitations.

Geologic background

The Maui field is one of the largest gas fields in New Zealand. Currently, OMV New Zealand owns and operates the field after acquiring it from Shell Exploration NZ at the end of 2018. Maui covers approximately 1000 km² and is located 40 km off of the West coast of the North Island (Figure 1) in approximately 100 m water depth (Pannett et al., 2004). The field comprises large low-relief anticlines that form the Maui A region in the northeast and the Maui B region in the southwest. The field produces from northeast–southwest-trending fairways of Paleocene to Eocene-aged, stacked marginal marine to terrestrial sandstone reservoirs, called the F, D, and C Sands (Pannett et al., 2004). The C Sand reservoir can be divided into C1, C2, and C3 intervals, although most of the gas-condensate reserves in the Maui field are stored in the C1 Sand (Bryant et al., 1995; Pannett et al., 2004). This study focuses on the C1 Sand reservoir that is composed of middle Eocene-aged lower coastal plain to inner shelf sediments that form laterally continuous, high net-to-gross reservoirs within the Maui field. A thin shale unit in the Maui B region, which is correlated to a carbonate-cemented unit in Maui A, serves to subdivide the C1 Sand reservoir into C1U and C1L (Bryant et al., 1994, 1995). The thickness of each sand is 15–30 m. In this study, we name the middle unit “C1M” that divides the C1 Sand reservoir into C1U (C1 Upper) and C1L (C1 Lower).

Field history and 4D interpretation

The field was discovered in 1969. The Maui-1 well penetrated the Maui B region, and the Maui-2 and Maui-3 wells penetrated the Maui A region. Production began in Maui A through 14 wells that were drilled from a single platform. Three more appraisal wells were drilled in 1986, and 1600 km² of 2D seismic data were acquired (Pannett et al., 2004). In 1990, water breakthrough in the Maui A wells showed that the field was producing under a stronger water drive than expected. A full-field 3D seismic survey was acquired in 1991 to assist in the development of the Maui B region (Figure 1). In 1993, Maui B was put on production with 10 wells drilled from a single platform. Water breakthrough in the MB-09 well indicated more severe water overrun that was not explained by the 1995 and 1997 updated reservoir models. In addition, these models could not explain the absence of water in MB-12 (Pannett et al., 2004). These well

results indicated that the sweep mechanism in Maui B was more complicated than previously thought. Thus, a 4D seismic survey was acquired at Maui in 2002 that aided in updating the reservoir model and understanding reservoir performance (Pannett et al., 2004). This survey was followed by drilling campaigns in the Maui A and Maui B regions to recover bypassed hydrocarbons (e.g., Telford and Murray, 2008; Murray, 2010; Murray et al., 2010; Thangam, 2013). In 2018, another 4D seismic survey was acquired over Maui to monitor the reservoir production since 2002. According to the latest reserve estimates published by the Ministry of Business, Innovation, and Employment (MBIE) in 2019, the estimated remaining gas reserves of the Maui field are 99 billion cubic feet (BCF) and the estimated remaining oil reserves are 4.5 million barrels.

Data set

As previously noted, three 3D seismic surveys have been acquired over the Maui field. The first seismic survey, shot in 1991, serves as the 4D baseline and covers 1000 km² (Figure 1). It was acquired in a quad-quad configuration using two boats, each with two streamers and two sources. The shot interval was 18.75 m, and the receiver group interval was 25 m. For technical and economic reasons, replication of the 1991 survey parameters was not possible. However, a test swath of single-vessel data acquired in 2001 showed a strong 4D signal at the reservoir level and acceptable repeatability (Pannett et al., 2004). The second seismic survey (monitor 1) was shot in 2002. It covers 480 km² and was acquired with a single boat using two sources and six streamers with 18.75 and 12.5 m shot and receiver group intervals. A 2 ms sample rate was used (Van der Veenken, 2016).

During the acquisition of the monitor seismic data, the Maui A and Maui B production platforms were in place. To ensure the safety and integrity of the platforms, a 500 m exclusion zone was enforced around the production facilities that created gaps in the monitor seismic data (Pannett et al., 2004). The third seismic survey (monitor 2) replicated the 2002 seismic program and was acquired in 2018 (McConnell and Pannell, 2018). However, only the 1991 3D and 2002 4D seismic data have been released for research by the MBIE, New Zealand. The 1991 and 2002 seismic data were coprocessed by Shell New Zealand in 2008 (R. Swift, personal communication, 2020). These reprocessed data are

used in this study. The released data are in the time domain with a 2 ms sample rate. The data quality and repeatability are very good with a normalized root-mean-square (rms) value of less than 0.2 (supplemental information can be accessed through the following link: Figure S1). However, only the full-stack data were made available. We do not have access to partial-stack data.

Sixty-nine wells have been drilled in the Maui field, and most of their data were released for research. However, only 23 wells have conventional well logs (bit size, caliber, gamma-ray, density, neutron, resistivity, and sonic logs), well completion reports, and deviation surveys. Only the well completion reports and deviation surveys are available for the rest of the 42 wells used in this study. Production data for some wells were also released. Some wells were drilled long after the monitor

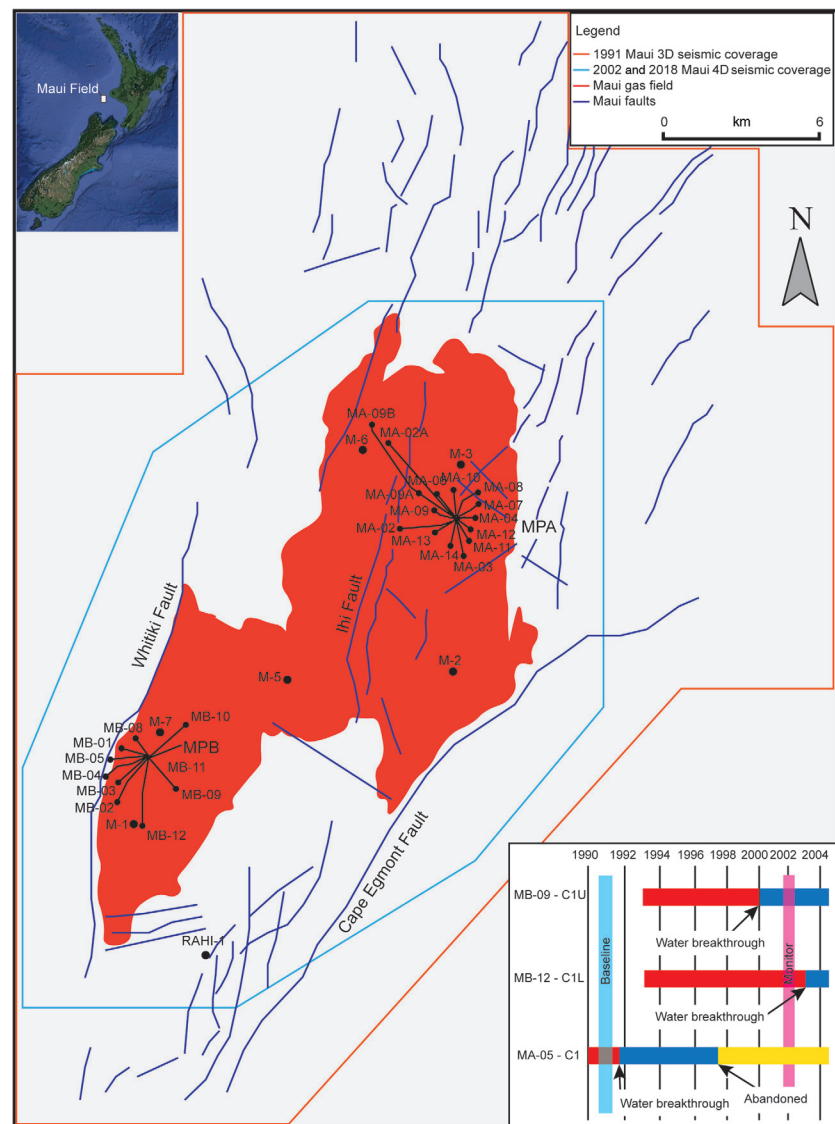


Figure 1. Location map of the Maui field in Offshore Taranaki Basin, New Zealand (modified from Google Earth, Pannett et al. [2004] and Van der Veenken [2016]). MA, Maui A wells; MB, Maui B wells; MPA and MPB, Maui A and B production platforms; and M, Maui vertical exploration wells.

survey was acquired, and others were drilled in the data gaps. Thus, not all wells were used in the study.

Methods

Figure 2 shows the workflow implemented in this study. We start with the qualitative interpretation of the C1 Sand reservoir. We perform seismic-to-well ties of the baseline and monitor surveys to identify the main seismic events, which include the C1U and C1L intervals, and to get accurate time/depth relationships for machine-learning analysis. For 4D studies, it is essential to ensure that the same attribute parameters and SOM models are simultaneously used in the analysis of the baseline and monitor. Thus, the position of the monitor data is translated to the east so that the baseline and monitor data (i.e., seismic and horizons) can be included in single files. Well data are also copied to the new monitor seismic location.

We compute typical instantaneous and spectral decomposition attributes sensitive to reservoir thickness and to changes in reservoir properties in the C1 Sand reservoir levels on the baseline, monitor, and difference volumes. We use visual analysis and principal component analysis (PCA) to select the attributes that best show 4D changes that agree with the production data and the amplitude difference volume. These attributes are then used as the input for SOM analysis. The SOM classification volumes are correlated to the well data to determine if the clusters can discriminate wet sand from hydrocarbon-charged sand and shale. If the SOM clustered volume satisfies these conditions, then we study the clusters using vertical sections and 3D views. The SOM classifications are correlated to the amplitude difference and production data to identify swept and unswept areas of the reservoir.

Finally, geobodies are extracted from meaningful baseline and monitor SOM clusters. Recoverable

gas volumes are computed for those geobodies. The difference in the recoverable gas associated with the SOM-derived geobodies is compared to the gas volume computed from geobodies extracted from the quadrature amplitude difference and to the production data.

4D interpretation

The 4D interpretation of the baseline, monitor, and difference volumes aids in identifying the fluid changes that occurred between 1991 and 2002 due to production from the C1 Sand reservoir. Gassmann fluid (Gassmann, 1951) substitution modeling suggests that a water sweep of the gas results in a 4% increase in acoustic impedance, driven mostly by the density change. Rock-physics models show that the effect of pressure depletion on velocity is small (<1%) (Hussein, 2020). Seismic wedge models show that tuning occurs for reservoir thicknesses of approximately 20 m (supplemental information can be accessed through the following link: Figure S2).

Figure 3a and 3b shows vertical sections intersecting the MB-12 well and extracted from the baseline and monitor seismic volume. Figure 3c displays the quadrature difference (monitor-baseline) after cross-equalization. Time shifts between baseline and monitor are calculated using a Taylor expansion algorithm (Naeini et al., 2009). The vertical section extracted from the time-shift volume (Figure 3d) shows very small time-shift values (less than ± 1 ms) that align with the shooting direction and are thus likely the result of subtle acquisition and processing differences between the baseline and monitor seismic volumes. The figure does not appear to show production-related time shifts.

The difference section (Figure 3c) shows two seismic peak events that indicate increases in impedance over time (hardening). This is likely to have been caused by water replacing gas or by pressure depletion in the C1U and C1L reservoir intervals. The MB-12 well was completed in the C1L and put into production in 1993. Time-lapse logging of MB-12 shows a gradual water-bottom rise in the high-quality C1L sand (Pannett et al., 2004). The impedance hardening observed in the C1U sand suggests flank water override as water replaces gas because of production in other Maui B wells. This was confirmed by time-lapse saturation logging acquired in MB-12 in 2003 (Pannett et al., 2004).

The rms average amplitude map over the reservoir interval (Figure 4a), extracted from the difference volume for the C1U reservoir interval, shows impedance hardening (the cyan to orange colors) in the Maui B and Maui A regions. The C1 Sand reservoir produces under a strong water drive that

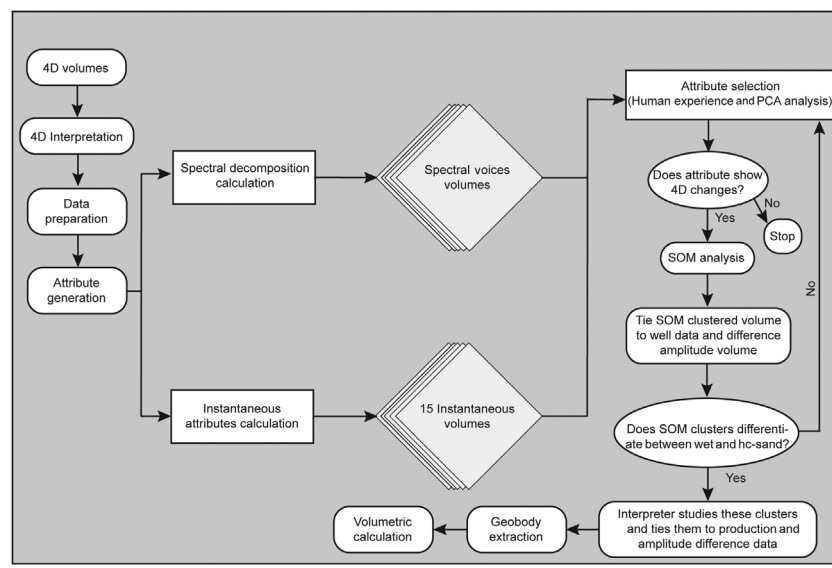


Figure 2. Attribute selection and SOM cluster analysis workflow implemented in this study.

comes from aquifers to the southeast and from the west across the Whitiki anticline (R. Swift, personal communication, 2020). Clearly, 4D changes at Maui B are larger than the 4D signal at Maui A. This is because much of Maui A's gas production was prior to the acquisition of the baseline survey in 1991. Production data (Figure 1) for two Maui B wells (MB-09 and MB-12) and one Maui A well (MA-05) suggest that larger gas volumes were withdrawn from the Maui B wells compared with Maui A wells between 1991 and 2002.

Seismic attribute selection

In the absence of angle stacks/gathers, we focus on poststack seismic attributes, such as spectral decomposition and instantaneous seismic attributes, that are sensitive to lithologic and reservoir property changes in addition to reservoir thickness variations. Spectral decomposition attributes measure the time-varying spectral properties of the seismic data. These spectral properties include spectral magnitude components, spectral voice components, peak frequency, peak magnitude, tuning frequency, and spectral bandwidth (Barnes, 2016; Marfurt, 2018). Instantaneous attributes are defined as time-frequency attributes, which are computed sample by sample on the real and quadrature components of the analytic seismic trace (Taner, 2001; Chopra and Marfurt, 2007).

We usually interpret broadband seismic data. However, broadband data may not be the optimal input to seismic attribute analysis because some spectral bands can be contaminated by noise (Li and Lu, 2014). Investigating the frequency spectrum of the original amplitude 4D data of the Maui field shows that the lower frequencies are contaminated by noise and the higher frequencies are less repeatable (supplemental information can be accessed through the following link: Figure S3a). Spectral decomposition analysis maps a 1D signal to a 2D signal of time and frequency, which results in different spectral amplitude and phase components (Partyka et al., 1999; Castagna et al., 2003). Analyzing these various spectral components enables selection of the ones closest to the tuning frequency of the reservoir and eliminate those bands that are contaminated by noise (White et al., 2015). We calculate the spectral decomposition attributes of the baseline and monitor seismic volumes by using the continuous wavelet transform. We perform spectral decomposition analysis at the reservoir interval for a frequency range of 10–70 Hz. The spectral difference volumes are then calculated by subtracting the spectral baseline from the spectral monitor data. The aim of this analysis is

to select a spectral voice (frequency band) that is close to the tuning frequency of the reservoir. A visual analysis of the calculated quadrature phase of the spectral difference volumes, based on the amplitude and signal to noise, shows that the reservoir tuning frequency lies

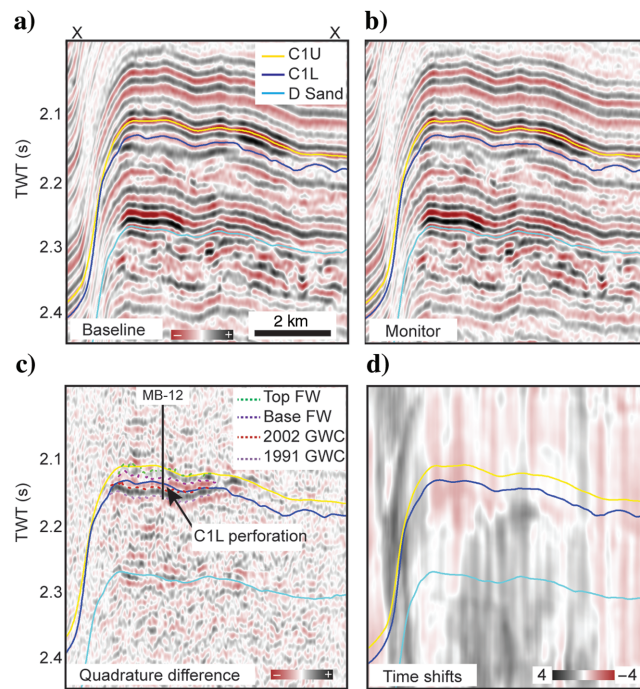


Figure 3. Vertical seismic sections crossing the MB-12 well extracted from (a) the zero-phase baseline, (b) monitor, (c) quadrature difference, and (d) time shift volumes. The amplitude range for the baseline and monitor seismic is ± 5000 and for the quadrature difference, it is ± 1500 . The location of the vertical sections is shown in Figure 4.

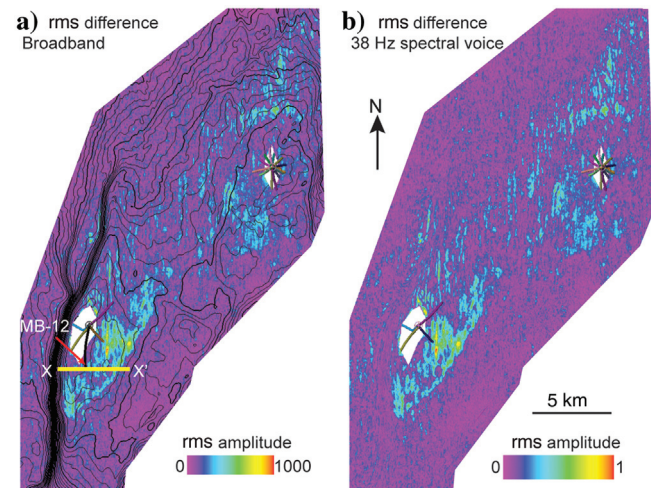


Figure 4. The reservoir interval rms amplitude map for the C1U reservoir calculated for (a) the broadband amplitude difference and (b) the 38 Hz spectral voice amplitude difference. The lines in (a) show all wells that were producing between 1991 and 2002. The red arrow refers to the MB-12 well path. The yellow line X-X' shows the location of the vertical cross sections displayed in Figure 3.

between 30 and 50 Hz, within which the 4D changes are best observed. However, visually analyzing the resultant spectral components to determine which frequency bands contain the most information about the reservoir is challenging. As a result, we turn to statistical analysis to enable us to select the spectral frequency that best represents the reservoir tuning frequency, which may contain the most information about the reservoir.

PCA is a linear statistical technique that can distill an enormous library of seismic attributes into a smaller set of seismic attributes based on the relative variance of the attributes within the interval of interest (Roden et al., 2015). We run PCA analysis on 11 spectral voices (frequency bands) of the baseline volumes, which are generated using spectral decomposition from 30 to 50 Hz in a window 10 ms above to 70 ms below the mapped C1U reservoir horizon. Investigating the PCA results, we find that the 38 Hz spectral voice is listed on top of the other attributes included in the first eigenvector with a 9.25% contribution (supplemental information can be accessed through the following link: Figure S4). This shows that the 38 Hz spectral voice ac-

counts for most of the variance within the data and is close to the tuning frequency of the reservoir. The rms amplitude map over the reservoir interval, calculated from the difference of the 38 Hz spectral voice of the baseline and monitor volumes (Figure 4b), shows 4D changes similar to those illuminated by the broadband difference amplitude volume (Figure 4a). However, the rms difference of the 38 Hz spectral baseline and monitor looks slightly cleaner compared to the broadband rms difference. The frequency spectra of the 38 Hz spectral baseline and monitor data show good 4D repeatability (supplemental information can be accessed through the following link: Figure S3b).

We computed 15 instantaneous attributes of the broadband and 38 Hz spectral baseline and monitor volumes. Here, we discuss the results for relative acoustic impedance, which calculates a running sum of the seismic traces and then applies a high-pass Butterworth filter. It is a modified version of recursive inversion described by Russell (1988) and Barnes (2016). This attribute can be considered as band-limited acoustic impedance and can help define discontinuities and be related to reservoir properties. Figure 5 shows a comparison between the relative acoustic attributes calculated for the broadband and 38 Hz spectral voice data using reservoir-interval attribute extractions for the C1U reservoir. The white polygons show data gap underneath the Maui A and B production platforms. A reservoir interval extraction from the relative acoustic impedance baseline (Figure 5a) shows large negative amplitudes that suggest deposition of low-impedance sands in Maui A and Maui B. The monitor relative acoustic impedance slice (Figure 5b) shows slightly lower amplitude values in the eastern and southern parts of Maui B and the southern side of Maui A (the orange arrows). This increase in relative impedance is likely to have been caused by production from the C1U Sand reservoir.

We compare broadband relative acoustic impedance reservoir slices (Figure 5a and 5b) with those same attributes calculated from the 38 Hz spectral voice baseline and monitor volumes (Figure 5c and 5d). The attributes computed from the 38 Hz spectral voice, which we call spectral instantaneous attributes, show more details than those calculated from the broadband seismic data. The spectral relative acoustic impedance attributes better illuminate the sandy facies in the western part of Maui A and the channelized sand-filled features (the white arrows) in the saddle between Maui A and B compared with those instantaneous attributes calculated from the broadband data. In addition, the sheet-like sandy facies deposited in Maui B north (the cyan arrow) are better illuminated on the spectral attributes compared with the broadband instantaneous attributes. However, these sheet-like facies seem to be better imaged in the monitor seismic compared with the baseline. This suggests that the monitor data have slightly better quality compared with the baseline in this area. Like the broadband instantaneous attributes,

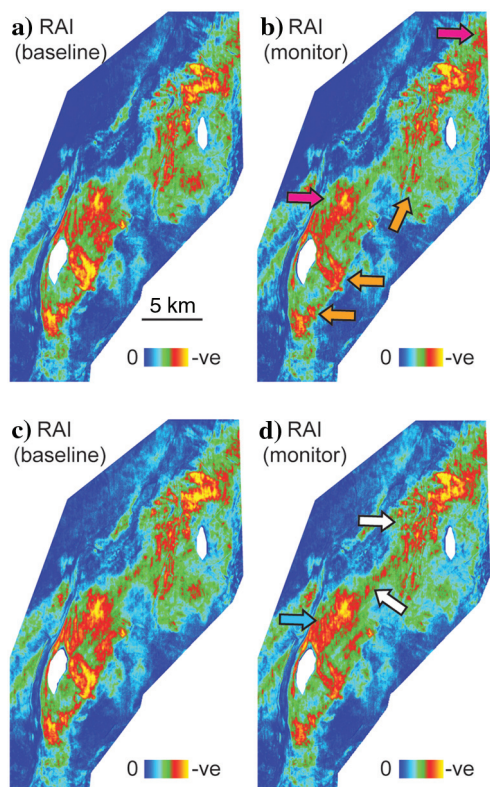


Figure 5. C1U reservoir interval slices extracted from (a and b) the broadband RAI attribute and (c and d) the 38 Hz spectral RAI. The white polygons show data gap zones underneath the Maui A and B platforms. The orange arrows show areas with reduced amplitudes observed in the monitor survey. The white and cyan arrows refer to areas where the sandy facies are better illuminated in the spectral RAI slices compared with the broadband RAI slices. The pink arrows refer to reservoir facies that are better imaged on the monitor data compared to the baseline data.

the spectral instantaneous attributes show decreased values in Maui B to the south and east and in Maui A to the south that suggest water sweep in these areas. Therefore, the spectral instantaneous attributes can be useful candidate attributes for machine-learning analysis of 4D seismic data.

Unsupervised machine learning for 4D seismic studies

The SOM is an unsupervised machine-learning technique that can efficiently extract similar natural clusters within multiple seismic attribute volumes and project those similar patterns into one classification volume (Strecker and Uden, 2002; Roy et al., 2011; Zhao et al., 2016). SOMs use a nonlinear neural network to perform a sample-based investigation of the various input normalized seismic attributes in a multidimensional attribute space (Coléou et al., 2003; Roy et al., 2013; Roden et al., 2015). SOMs are sensitive to subtle variations within the input seismic attributes (Roy et al., 2011). Using a 2D topology map, the SOM groups or clusters similar data together into one clustered volume. The SOM clusters are topologically ordered with similar clusters lying beside each other within this 2D map (Roy et al., 2013). The user can control the number of natural clusters based on the predefined number of neurons within the 2D map (Kohonen, 1982; Matos et al., 2006).

The previous discussion focused on the analysis of spectral decomposition and instantaneous attributes, extracted from baseline and monitor seismic volumes, to understand their sensitivity to 4D changes. For the SOM analysis, we ensure that the same SOM training model is applied to the baseline and monitor. Thus, variations in the SOM clusters' shapes or colors can be tied to production-related changes at the reservoir level. We expect to observe very similar clusters in the baseline and monitor data in areas with no production.

To select the attributes for SOM analysis, we visually analyze 15 spectral instantaneous attributes, looking for differences between the baseline and monitor volumes. We then apply a PCA analysis at the reservoir level and select those attributes that are prominent in the first three eigenvectors (supplemental information can be accessed through the following link: Figure S5). Combining the two analyses, the spectral instantaneous frequency, spectral thin bed, spectral quadrature component, spectral relative acoustic impedance, spectral sweetness, spectral envelope, spectral attenuation, and spectral cosine of instantaneous phase attributes (supplemental information can be accessed through the following link: Figure S6) are selected as input for unsupervised machine learning. All input attributes are normalized so that no one attribute has more weight than another.

In the first step of machine-learning analysis, SOM neurons (called prototype vectors in some publications) are trained using the eight spectral instantaneous attributes extracted from the baseline volume within the interval 10 ms above to 70 ms below the top of

the C1 Sand reservoir. The training is done at the seismic sample scale to gather similar data within the 8D attribute space into distinct natural clusters. Then, the trained winning neurons are used to classify all of the multiattribute seismic samples in the baseline and monitor volumes. This ensures that the same clusters on the baseline and monitor classification volumes have the same geologic meaning. The natural SOM clusters are projected using an 8×8 topology map. The baseline and monitor SOM volumes are then correlated to well data, and a 3D volumetric interpretation is performed on the classification volumes to visualize swept versus undrained areas.

SOM for reservoir monitoring

Like the wiggle trace display of a 4D seismic amplitude volume, SOM natural clusters of seismic attributes do not have an explicit geologic or production meaning on their own. They are patterns within the input seismic volumes that can then be correlated to geology and reservoir properties. Therefore, SOM clusters are correlated to well data, production information, and 4D seismic difference attributes using vertical and 3D displays. The first step is to correlate the SOM clusters of the baseline and monitor surveys to exploration and appraisal wells to validate that the SOM clusters are nearly the same where no production has occurred. Figure 6 shows a well display for three exploration and appraisal wells that penetrated the C1 Sand reservoir. The display shows the original wireline logs, petrophysical logs, flow units (Hussein et al., 2021), and SOM classifications extracted from the baseline and monitor volumes. The SOM classification volumes resolve thin beds down to ≈ 4 m thick. These are below the seismic resolution (a tuning thickness of ≈ 20 m). Maui-7 was drilled in Maui-B. Maui-5 targeted the saddle between Maui A and B, and Maui-6 penetrated the more distal part of the field to the west of Maui-A. Maui-7 is close to production wells in an area likely affected by production. The other two wells are far away from Maui A and B production wells in areas unlikely to be affected by production. Thus, the SOM clusters extracted along Maui-5 and Maui-6 from the baseline and monitor classification volumes are very similar (Figure 6). For instance, at Maui-5, nearly the same SOM clusters/neurons (N46 and N47) are observed for the C1U sand in the baseline and monitor SOM volumes. This helps validate repeatability of the baseline and monitor SOM classifications and suggests that any variations in the SOM clusters close to or at producing wells could be correlated to production-related changes (i.e., water saturation changes).

Maui-7 is an appraisal well located on the northern edge of the data gap associated with the production platform at Maui B. Unfortunately, no data from production wells outside of the gap zone are available. However, because of its proximity to production wells, we expect some production-related changes to be observed at or close to Maui-7. Using the Maui-7 well to

analyze the baseline SOM classification volumes, the gas-charged sand of the C1U interval shows baseline SOM clusters (N32, N40, N48, N58, and N61) that are distinctly different from those observed in the gas-charged sand of the C1L (N39, N47, N54, and N53). Those gas-charged sand baseline SOM clusters are also different from the C1M clusters (N5, N16, N15, N24, and N31). This suggests that the SOM is sensitive to subtle rock property changes within the reservoir (Figure 6).

In C1U and C1L, unlike in Maui-5 and Maui-6, the baseline and monitor clusters are different. This is expected because of production from wells close to Maui-7. We will discuss this in the next paragraph. However, in the C1M interval, composed of shale and silty shale, there also slightly different baseline and monitor SOM clusters (Figure 6). These thin intrareservoir shale units seem to be hydrocarbon charged. The changes in the cluster patterns could be caused by water replacing gas even though the shales have relatively low permeability. In addition, these shales can respond to pressure changes within the surrounding sands (about a 15% decline compared to the initial reservoir pressure; Pannett et al., 2004). This can cause subtle time shifts (MacBeth et al., 2011; Rangel et al., 2016) that are possibly detected by the SOM classification.

Based on rock quality analysis (Hussein et al., 2021), the C1 Sand reservoir can be divided into different flow units (Figure 6). At the Maui-7 well, 11 flow units are identified. Flow units 2, 4, 7, 8, and 10 are high-speed reservoir flow units with very good reservoir quality. Flow units 3, 6, and 9 are normal reservoir flow units with moderate to good reservoir quality. Flow units 1, 5, and 11 are baffles with poor reservoir quality or nonreservoir facies (Figure 6). Baffles are defined as zones that throttle fluid movements, which comprise poor-quality reservoir and/or nonreservoir facies. The SOM classifications correlate well to flow units. For instance, the baseline SOM clusters N32, N61, N5, N16, N15, N24, and N31 are correlated to baffles. The N40, N48, N47, N54, N53, and N4 clusters are correlated to high-speed and normal reservoir flow units. We find that the SOM is useful in monitoring water saturation changes in the good reservoir units. But the SOM can also help monitor poor-quality reservoirs, changes in which cannot be observed in 4D amplitude volumes. The monitor SOM classification shows slightly different clusters compared with those observed in the baseline SOM. For example, the monitor SOM shows that N20 correlates to the gas-charged poor-quality reservoir within baffle FU1, whereas the baseline SOM shows

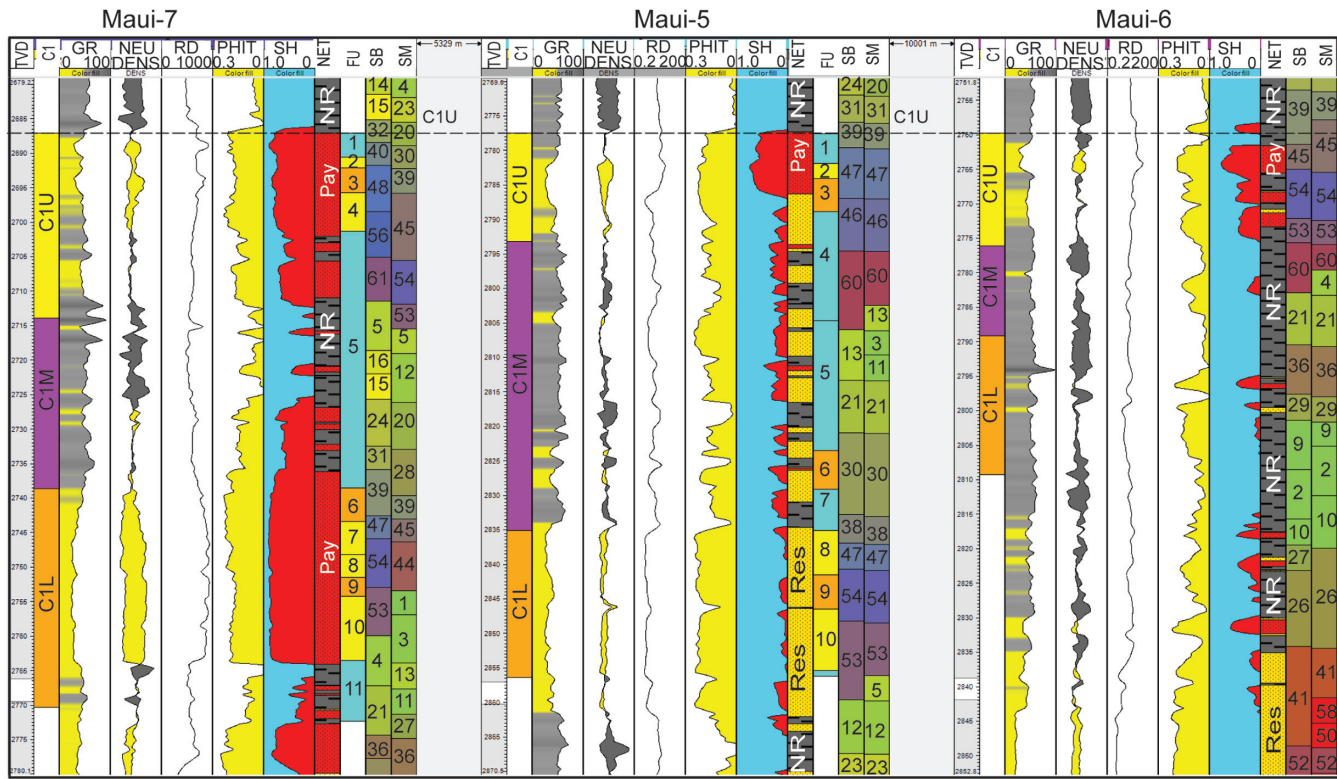


Figure 6. Well section display for three vertical Maui wells showing wireline logs, petrophysical logs, and flow units. Also shown are SOM classifications for the baseline and monitor surveys extracted at the well locations. GR, gamma ray; NEU, neutron; RD, deep resistivity; PHIT, total porosity; SH, hydrocarbon saturation; Pay, net pay; Res, net reservoir; NR, nonreservoir; FU, flow units; SB, SOM baseline; and SM, SOM monitor. The FU track shows the flow unit numbers defined by Hussein et al. (2021). The SB and SM tracks indicate the neuron numbers from the SOM classification volumes. The yellow and orange flow units indicate high-speed and normal reservoir flow units, respectively, whereas the cyan ones indicate baffles.

that N32 correlates to the same unit at the Maui-7 well (Figure 6). This suggests that the C1U sand reservoir flow units have been water swept, and the different monitor SOM clusters reflect the change in seismic response produced by water replacing gas.

Investigating the SOM classification of the baseline and monitor volumes using vertical and 3D views enables us to identify swept areas of the reservoir and locate the undrained parts. Figure 7a shows a vertical section extracted from the baseline SOM classification volume, corendered with the quadrature component of the baseline seismic data. The section crosses the Maui-7 well, on which the net pay discrete log is displayed. The SOM classification volume shows more details in the seismic facies compared with the quadrature component data. At the well location, the baseline SOM clusters N32, N40, N48, N56, and N61 (denoted by the red circles in the SOM topology map of Figure 7a) are correlated to gas-charged sand in the C1U reservoir. These clusters pinch out updip and extend to touch other blue clusters to east of the well (N62, N63, and N64; denoted by the orange circles in the SOM legend of Figure 7a). These blue clusters lie beside the gas-charged clusters in the SOM topology map, suggesting similar reservoir properties. In addition, the quadrature component response of these clusters shows a strong negative amplitude, suggesting gas-charged sand.

The same vertical section extracted from the monitor SOM volume and corendered with the quadrature component of the monitor seismic data is shown in Figure 7b. Clusters N20, N30, N39, N45, and N54 (denoted by the red circles in the SOM cluster legend of Figure 7b) are correlated to the C1U sand at Maui-7 but differ from the clusters observed in the baseline survey. This suggests that the reservoir has been swept at the Maui-7 location because of production from nearby wells located at the crest of the Maui B structure. However, we cannot know whether the reservoir has been fully or partially swept. The only way to find out would be to drill a new well that penetrates these clusters, to acquire a repeat saturation log at the Maui-7 well or apply 4D elastic inversion to estimate the density change, if angle stack data were to become available. Clusters N62, N63, and N64 are also observed in the monitor SOM volume, which suggests that these are unswept areas of the C1U reservoir.

Figure 8 shows 3D views of the baseline and monitor SOM clusters for the C1U sand reservoir and production wells that were producing from the reservoir between 1991 and 2002. Figure 8a shows the C1U classification volume with all neurons turned on. The figure shows that nearly the same SOM clusters are observed in both surveys at the edges of the field where shelfal shale is deposited. However, there are subtle changes in the cluster patterns between the baseline and monitor SOM volumes over the Maui A and Maui B regions. Figure 8b shows cluster N32, which is correlated to gas-charged poor-quality reservoir within FU1 at the Maui-7 well (Figure 6). This cluster shows a smaller areal extent in the monitor SOM volume compared with the baseline SOM, which suggests that the

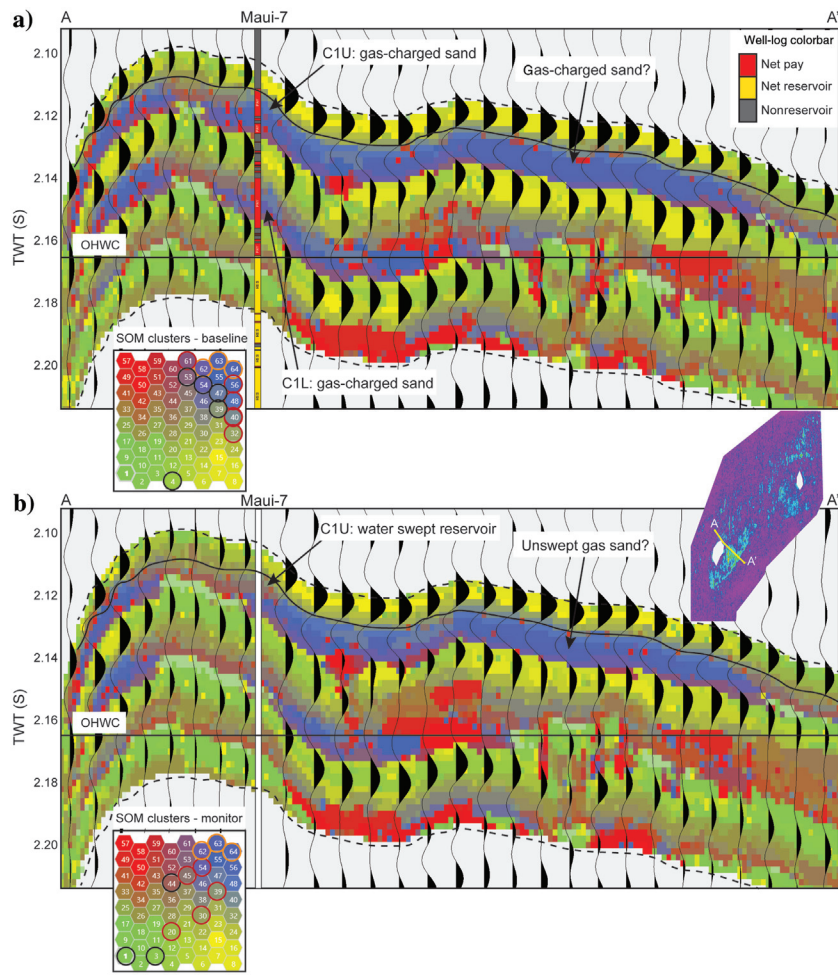


Figure 7. Vertical sections extracted from SOM classifications corendered with the quadrature phase components of the (a) baseline and (b) monitor volumes. The sections intersect the Maui-7 well, which in (a) displays a discrete log of net pay and net reservoir. The red and black circles around neurons in the SOM topology map indicate SOM clusters in C1U and C1L that are correlated to gas-charged sands at the Maui-7 well. The orange circles are interpreted as neurons showing the extension of C1U sand to the east of the Maui-7 well. The approximate original hydrocarbon water contact (OHWC) is shown as a flat line, but, in reality, it is likely not flat in two-way traveltime (TWT). The inset is the rms amplitude map for the C1U reservoir extracted from the broadband difference amplitude volume showing the vertical section location. The white bar in (b) indicates the well location where we have no well-log data at the time of the monitor data (2002).

reservoir has been partially swept. In addition, this cluster is not seen at the Maui-7 well. However, N32 in the northern part of Maui B covers a slightly larger area in

the monitor SOM (the orange arrow in Figure 8b) compared to the baseline. This observation, which is likely because of better imaging in the monitor survey, agrees

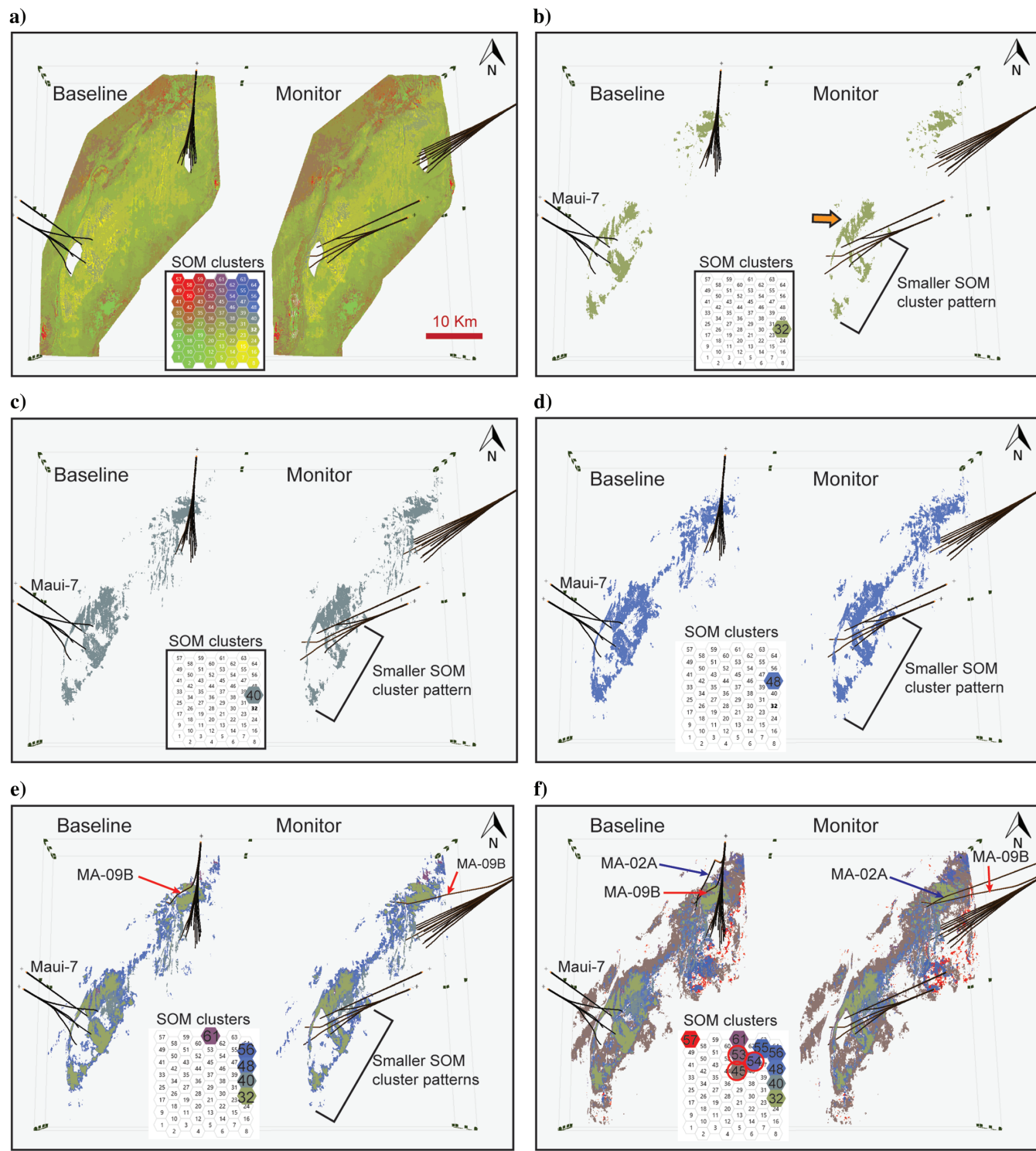


Figure 8. A 3D view of SOM clusters for the upper C1U Sand reservoir (a) with all clusters displayed and SOM clusters correlated to gas-charged flow units at Maui-7 well (b-d). (b) Neuron N32 that is correlated to the poor-quality reservoir within baffle FU1, (c) N40 that is correlated to moderate- to very good quality reservoirs, and (d) N48 that is correlated to high-speed and normal reservoir flow units. Gas-charged SOM clusters penetrated by the (e) Maui-7 and MA-09B wells and (f) Maui-7, MA-02A, and MA-09B and N55 and N57, which show changes in SOM clusters in Maui A south. The orange arrow in (b) shows a slightly larger reservoir cluster in the monitor SOM compared to the baseline SOM, which agrees with the attribute slices displayed in Figure 4.

with the interpretation of the broadband and spectral instantaneous seismic attribute slices discussed earlier (Figure 5). The SOM cluster N40 (Figures 6 and 8c) is correlated to gas-charged, moderate- to very good quality reservoirs within FU1 and FU2 at the Maui-7 well, and it covers a slightly smaller area in the monitor SOM compared to the baseline. This suggests that the reservoir has been swept at Maui B east and south. The SOM cluster N48 (Figures 6 and 8d) is correlated to gas-charged high-speed and normal reservoir flow units at the Maui-7 well. This cluster shows a smaller areal extent in the monitor SOM compared to the baseline where the reservoir seems to be swept in Maui B east and south (Figure 8d).

The baseline SOM clusters correlated to the C1U gas-charged sand flow units at the Maui-7 well are displayed in Figure 8e. Those clusters seem to cover a smaller area in Maui B east and south and extend to the west side of Maui A where the MA-09B well, drilled in 2013, penetrated similar clusters (N40, N48, N56, and N63) to those defined at Maui-7. The MA-09B well found a thin gas sand (approximately 1 m in the C1U), but the rest of the gas sands in the well seem to have been swept by production from the MA-02A well (Thangam, 2015). The MA-02A well, drilled in 2006, penetrated the C1U Sand reservoir clusters (N45, N54, and N53) and found unswept gas with the original gas-water contact (Telford and Murray, 2008). Figure 8f shows a 3D view of the Maui-7, MA-09B, and MA-02A wells with the gas-charged reservoir clusters turned on (those circled in red on the SOM cluster legend). The reservoir clusters to the west side of Maui A seem to be connected and show the same patterns in the baseline and monitor SOM views.

To validate this observation, vertical sections extracted from baseline and monitor classifications and corendered with the corresponding quadrature-phase seismic volumes are shown in Figure 9. These sections intersect the MA-09B, MA-02A, and Maui-3 wells. The net pay and net reservoir discrete logs, calculated from the original wireline logs, are displayed for MA-02A and Maui-3. No wireline logs are available for MA-09B. The gas-charged reservoir SOM clusters at MA-02A (circled in red in the SOM cluster legend) are in good communication with gas-charged clusters (circled in orange) identified at MA-09B. Comparing the baseline and monitor SOM classifications (Figure 9a and 9b, respectively), the SOM patterns

look similar, although subtle changes are observed to the east and west of the MA-02A well. This suggests that there has been little or no production on the west side of Maui A between 1991 and 2002. When MA-02A was put on production in 2006, these gas-charged sands seemed to have been swept (Thangam, 2015). This suggests that the SOM clusters (N32, N40, N48, N56, and N61) were gas charged and unswept until sometime after 2002. The subtle changes in the baseline and monitor SOM clusters to the east and west of MA-02A well might have been caused by very small pressure depletion because of production from the Maui B region. Note that the baseline and monitor SOM clusters (N28, N39, and N46; circled in cyan) penetrated by the Maui-3 well look very similar to each other. Maui-3 is an exploration well that was drilled into the C1 Sand reservoir in 1970. It is approximately 2.2 km from the Maui

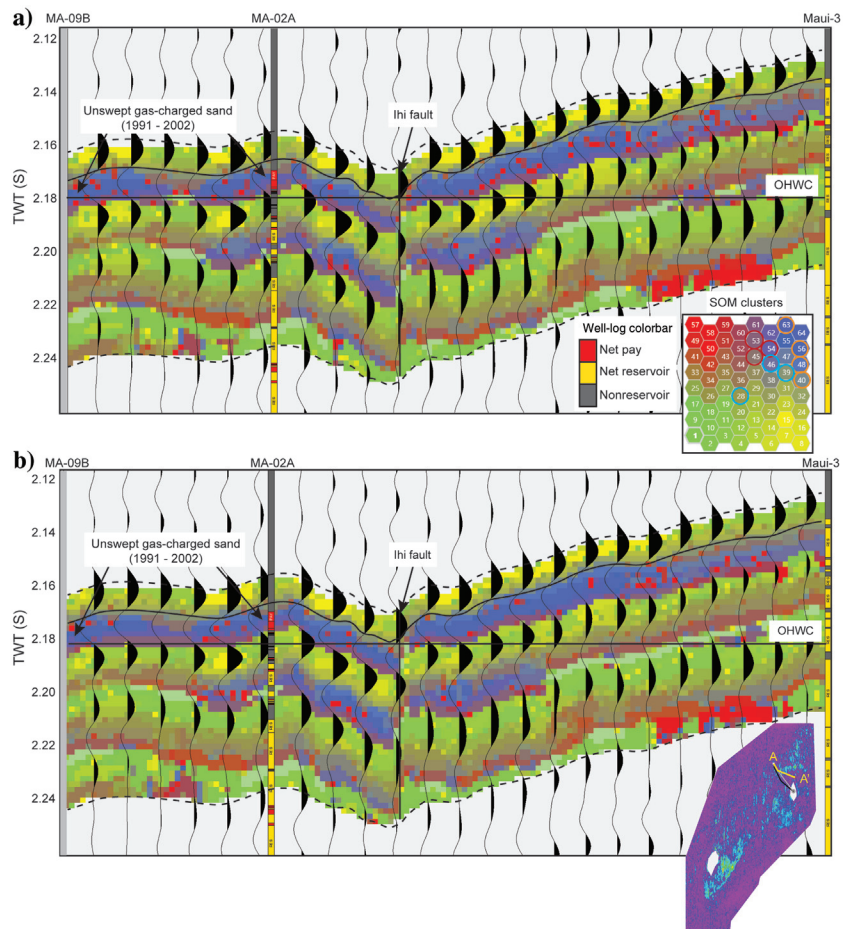


Figure 9. Vertical sections extracted from SOM classifications corendered with the quadrature phase components of the (a) baseline and (b) monitor volumes. These sections intersect the MA-09B, MA-02A, and Maui-3 wells, which display net pay and net reservoir discrete logs. No well logs are available for MA-09B. The black and white lines on the C1U rms difference inset map, extracted from the broadband difference amplitude volume, shows the MA-09B and MA-02A well paths, respectively. The orange and red circles around neurons in the SOM topology map show gas-charged sand reservoir penetrated by MA-09B and MA-02A wells, respectively. The cyan circles refer to the C1U Sand reservoir penetrated by the Maui-3 well. The approximate OHWC is shown as a flat line, but, in reality, it is likely not flat in TWT.

A production platform from which there had been significant production prior to the acquisition of the baseline survey in 1991. It is likely that the reservoir was swept or partially swept before the baseline survey was acquired. The similarity in clusters for the baseline and monitor surveys in this area suggests that little incremental production had occurred between 1991 and 2002. The gas-charged reservoir on the west of Maui A appears to be compartmentalized and sealed by the Ihi fault, which is likely to have prevented the gas from migrating updip toward the Maui-3 well (Figure 9).

Focusing on bottom water rise within the C1L reservoir interval, at the Maui-7 well the baseline SOM clusters (N39, N47, N53, N54, and N4) are correlated to gas-charged sand (Figure 7). However, the monitor SOM classification shows different clusters (N39, N45, N44, N1, and N3) in the C1L interval. This suggests that the C1L reservoir might have been swept by production

wells near Maui-7. Water breakthrough in 2003 was observed at MB-12 (Figure 1), just updip from Maui-7, validating this interpretation.

Figure 10 shows a vertical section that crosses the MB-12 well (drilled in 1993), extracted from the baseline and monitor SOM classification volumes and corendered with the quadrature components of the baseline and monitor data. The baseline and monitor SOM clusters are correlated to the gas-charged sands within the C1U Sand reservoir. The same clusters (N4, N31, N39, N45, N53, and N54; denoted by the orange circles in the SOM legend) are observed for the baseline and monitor SOM volumes. This suggests that there was little or no water sweep in the C1U Sand reservoir near the MB-12 well between 1991 and 2002. This agrees with the production data from this well.

On the other hand, the baseline and monitor SOM clusters look different for the C1L Sand reservoir. At the MB-12 well, there is a thin oil rim approximately 2 m thick. The oil rim is well below the seismic and SOM resolution, so it is hard to differentiate and/or resolve gas versus oil. In the baseline SOM classification volume, the C1L hydrocarbon-charged sands correlate to clusters N21, N28, N36, N41, and N1 and cluster N2 correlates to the hydrocarbon-water contact (Figure 10). For the monitor, the upper part of the C1L interval (gas-charged sands) is correlated to SOM clusters N28, N37, and N41, which are very similar to those observed in the baseline SOM volume. However, different clusters (N50 and N52) are observed in the lower part of C1L reservoir for the monitor SOM volume. This suggests that the lower part of the C1L interval might have been water swept. The monitor SOM classification clearly shows the change in the hydrocarbon-water contact. As the reservoir is being produced, the acoustic impedance in the reservoir increases because of the water sweep. Thus, the seismic response of the reservoir changes. This results in a change in the cluster patterns, which show a coning effect along the borehole and extending updip toward the rest of the production wells (Figure 10b). The monitor SOM volume shows cluster patterns along the borehole that cannot be imaged by the monitor seismic data or by the 4D amplitude difference. The red clusters may also be due in part to subtle changes in the seismic response because of pressure drawdown near the wellbore (Figure 10b).

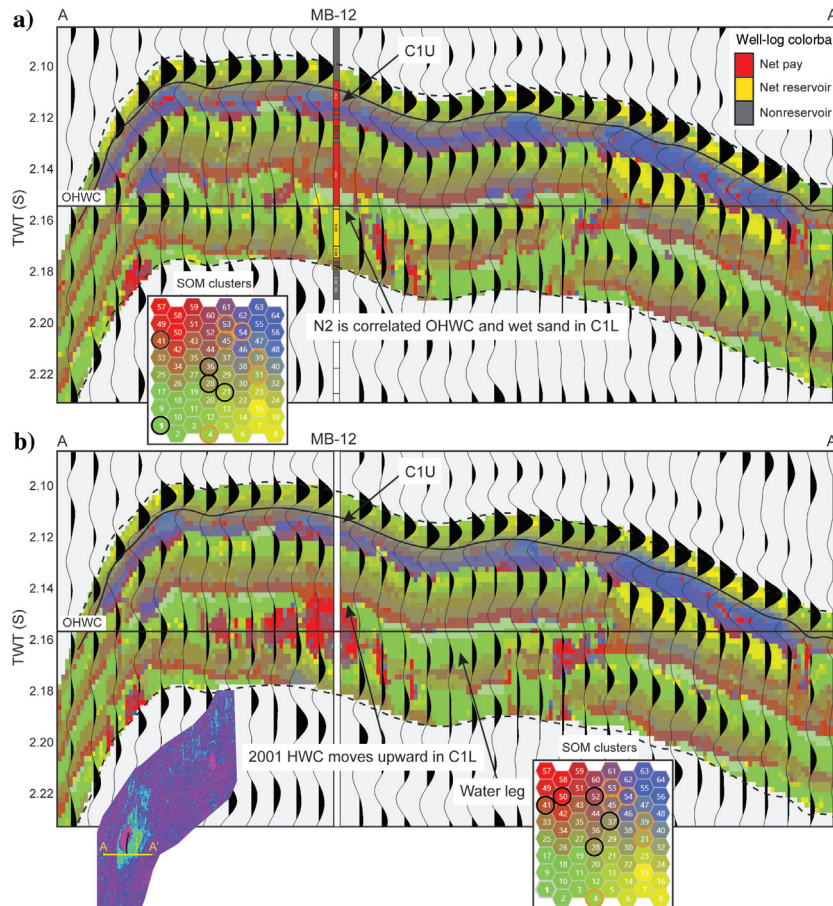


Figure 10. Vertical sections extracted from SOM classification corendered with the quadrature components of the (a) baseline and (b) monitor volumes. These sections intersect the MB-12 well, which in (a) displays net pay and net reservoir discrete logs. HWC refers to the hydrocarbon water contact. The orange and black circles around neurons in the SOM topology map indicate clusters that correlate to the C1U and C1L reservoirs. The approximate OHWC is shown as a flat line, but in reality, it is likely not flat in TWT. The inset slice is the rms amplitude for the C1L reservoir extracted from the broadband difference amplitude volume. The white bar in (b) indicates the well location where we have no well-log data at the time of the monitor data (2002).

Geobody extractions and volumetric calculations

In this study, we have shown a workflow that enables us to combine multiple seismic attribute volumes at a seismic-sample scale into SOM classification volumes. Analysis of the SOM cluster volumes facilitates the 4D interpretation of a reservoir below the tuning thickness (i.e., down to ≈ 4 m thick reservoir intervals). Geobodies can be created from SOM clusters that are tied to the well and production data. Once these geobodies are generated, the original hydrocarbon and recoverable gas volumes for the baseline and monitor conditions can be calculated by incorporating information from the wells that penetrate these geobodies.

The recoverable gas volumes for the baseline and monitor geobodies are calculated at Maui B. Baseline and monitor geobodies are generated using the SOM clusters identified at the Maui-7 well and those clusters that show a similar pattern but a reduction in size in the monitor classification compared with the baseline. Because of the lack of enough well control for calibration, we use average reservoir properties of the C1 Sand to calculate recoverable gas RG:

$$RG = GRV * N/G * PHI * (1-Sw) * GEF * RF, \quad (1)$$

where GRV is the gross rock volume of the geobody, N/G is the net-to-gross ratio (0.81), PHI is the porosity (0.18), Sw is the initial water saturation (0.25), GEF is the gas expansion factor (230), and RF is the recovery factor (0.6). The interval velocity used to convert the two-way time thickness of the geobody to depth thickness is 3635 m/s.

Calculating the size of the geobodies and their associated recoverable gas volumes for the baseline and monitor SOM volumes provides a quantitative measure of the amount of swept (and thus produced) hydrocarbon and the amount of remaining recoverable gas reserves (i.e., the unswept reservoir). The difference in the recoverable gas estimates between the baseline and monitor SOM geobodies is approximately 177 BCF. This result is smaller but on the same order of magnitude as an estimate of produced gas calculated from geobodies derived from the quadrature phase difference volume (252 BCF) and production data from the Maui B wells (416 BCF). This is expected in part because of missing data in the zone around the platform. There might also be other SOM clusters that are not included in the geobody extractions because of the lack of calibration wells.

Discussion

The SOM classifications of the baseline and monitor volumes are useful to monitor water sweep within thin reservoir intervals (below seismic resolution) of poor- and very good quality reservoir sands. Compared with the 4D amplitude difference volume, differences in the SOM classifications show more details that illuminate flank water override and changes in the hydrocarbon water contact. However, the baseline SOM classification

may not be useful in discriminating commercial gas-charged reservoirs from residual gas saturated reservoirs for the same geology. For example, in the C1L sand at the Maui-7 and Maui-5 wells, the baseline SOM classifies high-gas-saturated and low-gas-saturated, high-speed and normal reservoir flow units as N54 and N53 (Figure 6). Closer investigation of those flow units finds that they have the same facies (clean sand form estuarine channels) and similar porosity ranges between 18% and 21% (Hussein et al., 2021). However, at Maui-7, the monitor SOM shows different clusters (N39, N45, N44, N1, and N3) compared to the baseline SOM for the C1L interval. Similar baseline and monitor SOM clusters are observed at the Maui-5 well (Figure 6). This suggests that the 4D response may be more complicated than a water saturation change and may be caused in part by subtle pressure depletion.

Although SOM is an unsupervised machine-learning technique that classifies natural clusters within multiple input seismic attribute volumes, incorporating as many wells as possible in the interpretation process is vital. The absence of a logged well penetrating the C1 Sand reservoir in the Maui A region that is timed with either the 1991 or 2002 seismic data limits our understanding of the production-related changes in this area. Subtle changes in SOM cluster patterns are observed in the southern Maui A region (Figure 8f), but those clusters cannot be correlated to well data.

The data quality of the 4D seismic volumes controls the SOM classification results. The repeatability of the 4D seismic data of the Maui field is good. However, the 2002 monitor seismic data show slightly better imaging for the reservoir facies in Maui B north and the northern part of Maui A compared with the baseline volume (as illustrated by the pink arrows in Figure 5b). This results in SOM clusters that cover slightly larger areas in the monitor compared with the baseline volume (the orange arrows in Figure 8b), which are similar to the facies illuminated in the seismic attribute slices (the pink arrows in Figure 5b).

The spectral instantaneous seismic attributes show enhancements in illuminating subtle reservoir features (Figure 5) compared with the broadband data. The filtered 4D seismic data (i.e., 38 Hz) spectral baseline and monitor voices show better repeatability compared with the broadband seismic data (supplemental information can be accessed through the following link: Figure S3). However, computing seismic attributes on filtered data does not improve resolution but it does enhance the sensitivity to the reservoir changes.

Although the spectral quadrature component slice and the relative acoustic impedance (RAI) slice (supplemental information can be accessed through the following link: Figure S6) look similar to the result from a human interpreter, there are subtle differences observed in the RAI slice that are not shown in the quadrature component slice. These subtle differences seem to affect the SOM classification results. In addition, there are subtle differences (3%) statistically observed

between both attributes observed in the PCA (supplemental information can be accessed through the following link: Figure S5b). An example of how correlated attributes can impact SOM classification can be found in Hussein et al. (2021).

Only full-stack seismic volumes were available for this study, and only a few production wells were released for research. Thus, we were limited in terms of the available seismic data and wells that could be used to correlate and interpret baseline and monitor SOM classifications. The same workflow could be applied to seismic attributes extracted from partial angle stack data or to partial angle stack 4D difference volumes. Time-lapse well logs, if they were to become available, could be used to monitor changes in the hydrocarbon water contact or flank water override and would greatly assist SOM interpretation and calibration and might improve the predictable recoverable gas volumes. Also, undershooting the production platform (if it is economically possible) would aid in better recoverable gas estimation. In this study, water saturation changes dominate the 4D response of the C1 Sand reservoir. However, this method can also be applied to other reservoirs (e.g., those that are compacting) and using angle stacks as input to the SOM classification could possibly distinguish between saturation and pressure changes.

Conclusion

Time-lapse seismic attributes are often used to constrain the history match of reservoir simulation models, which are used to make better reservoir management decisions. Understanding reservoir heterogeneities and the associated 4D responses is a critical part of this process. In this study, we propose a machine-learning workflow that enables us to combine multiple spectral instantaneous seismic attribute volumes into merged classification volumes. Calibrating the SOM baseline and monitor classification volumes to well data, production data, and 4D seismic attributes helps to identify clusters that are meaningful in terms of production reservoir facies (swept versus unswept reservoir). Changes in the cluster patterns between baseline and monitor surveys suggest that production-related changes are primarily caused by water replacing gas. The 4D SOM classification volumes show internal reservoir heterogeneity and illuminate 4D changes for very good to poor-quality reservoirs and help us to identify thin baffles. Compared with the 4D seismic amplitude difference volume, 4D SOM volumes better show the changes in the flank water override and bottom water rise. Geobodies can be generated from the production-related SOM clusters of the baseline and monitor classifications. Computing recoverable gas volumes for the baseline and monitor geobodies and calibrating the difference in those volumes to production data aids in estimating the remaining recoverable gas. However, there are uncertainties in this calculation that cannot be fully addressed given this data set. SOM identifies natural

cluster patterns in multiple spectral instantaneous attribute volumes. However, determining the meaning of the clusters requires calibration using well data. Incorporating as many wells as possible is critical for accurate geobody extractions and volumetric calculations.

Acknowledgments

We would like to thank MBIE, New Zealand, for providing the data set containing the 3D seismic, well logs, and associated reports required for this study. Geophysical Insights and Schlumberger are greatly acknowledged for supporting the University of Houston with Paradise 3.2.3 and Petrel G&G software v.2019, respectively. Useful discussions with K. Marfurt, I. Mohamed, and E. Alfataierge are highly appreciated. Finally, we would like to thank T. Smith for commenting on an earlier version of the manuscript and for supporting the publication fees. M. Hussein and J. Wu acknowledge the computer workstation equipment purchased by the Governor's University Research Initiative provided by the State of Texas and the University of Houston. Publication fees were supported by Dr. Tom Smith and the Geophysical Insights company. We thank the reviewer A. E. Barnes and two anonymous reviewers for their constructive and helpful comments.

Data and materials availability

Data associated with this research are available and can be accessed via the following URL: <https://www.nzpam.govt.nz/>.

References

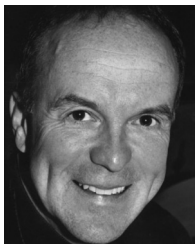
- Barnes, A. E., 2016, Handbook of poststack seismic attributes: SEG, SEG Geophysical Reference Series 254.
- Bryant, I. D., M. G. Marshall, C. W. Greenstreet, W. R. Voggenreiter, J. M. Cohen, and J. F. Stroeman, 1994, Integrated geological reservoir modelling of the Maui Field Taranaki Basin, New Zealand: New Zealand Oil Exploration Conference Proceedings, 256–281.
- Bryant, I. D., C. W. Greenstreet, and W. R. Voggenreiter, 1995, Integrated 3-D geological modeling of the C1 Sands reservoir, Maui Field, offshore New Zealand: AAPG Bulletin, **79**, 351–374, doi: [10.1306/8D2B152A-171E-11D78645000102C1865D](https://doi.org/10.1306/8D2B152A-171E-11D78645000102C1865D).
- Buland, A., and Y. El Ouair, 2006, Bayesian time-lapse inversion: Geophysics, **71**, no. 3, R43–R48, doi: [10.1190/1.2196874](https://doi.org/10.1190/1.2196874).
- Calvert, R., 2005, Insights and methods for 4D reservoir monitoring and characterization: SEG.
- Cao, J., and B. Roy, 2017, Time-lapse reservoir property change estimation from seismic using machine learning: The Leading Edge, **36**, 234–238, doi: [10.1190/tle36030234.1](https://doi.org/10.1190/tle36030234.1).
- Castagna, J. P., S. Sun, and R. W. Siegfried, 2003, Instantaneous spectral analysis: Detection of low-frequency

- shadows associated with hydrocarbons: The Leading Edge, **22**, 120–127, doi: [10.1190/1.1559038](https://doi.org/10.1190/1.1559038).
- Chopra, S., and K. J. Marfurt, 2007, Seismic attributes for prospect identification and reservoir characterization: SEG, SEG Geophysical Developments Series 452.
- Coléou, T., M. Poupon, and K. Azbel, 2003, Unsupervised seismic facies classification: A review and comparison of techniques and implementation: The Leading Edge, **22**, 942–953, doi: [10.1190/1.1623635](https://doi.org/10.1190/1.1623635).
- Doyen, P. M., 2007, Seismic reservoir characterization: An earth modelling perspective: EAGE Publications 256.
- Gassmann, F., 1951, Elastic waves through a packing of spheres: *Geophysics*, **16**, 673–685, doi: [10.1190/1.1437718](https://doi.org/10.1190/1.1437718).
- Gouveia, W. P., D. H. Johnston, A. Solberg, and M. Lauritzen, 2004, Jotun 4D: Characterization of fluid contact movement from time-lapse seismic and production logging tool data: The Leading Edge, **23**, 1187–1194, doi: [10.1190/1.1825941](https://doi.org/10.1190/1.1825941).
- Grana, D., and T. Mukerji, 2015, Bayesian inversion of time-lapse seismic data for the estimation of static reservoir properties and dynamic property changes: *Geophysical Prospecting*, **63**, 637–655, doi: [10.1111/1365-2478.12203](https://doi.org/10.1111/1365-2478.12203).
- Grochau, M., and P. Jilinski, 2016, 4D seismic spectral decomposition over a pre-salt carbonate reservoir: A feasibility study: 86th Annual International Meeting, SEG, Expanded Abstracts, 5547–5551, doi: [10.1190/segam2016-13870124.1](https://doi.org/10.1190/segam2016-13870124.1).
- Helgerud, M. B., A. C. Miller, D. H. Johnston, M. S. Udo, B. G. Jardine, C. Harris, and N. Aubuchon, 2011, 4D in the deepwater Gulf of Mexico: Hoover, Madison, and Marshall fields: The Leading Edge, **30**, 1008–1018, doi: [10.1190/1.3640524](https://doi.org/10.1190/1.3640524).
- Hussein, M., 2020, Machine learning for reservoir characterization and time-lapse seismic analyses: Ph.D. dissertation, The University of Houston.
- Hussein, M., R. R. Stewart, D. Sacrey, J. Wu, and R. Athale, 2021, Unsupervised machine learning using 3D seismic data applied to reservoir evaluation and rock type identification: *Interpretation*, **9**, no. 2, T549–T568, doi: [10.1190/int-2020-0108.1](https://doi.org/10.1190/int-2020-0108.1).
- Johnston, D. H., 2010, Methods and applications in reservoir geophysics: SEG, Investigations in Geophysics 2.
- Johnston, D. H., 2013, Practical applications of time-lapse seismic data: SEG, 130–146.
- Kleemeyer, M., P. Gelderblom, A. Altintas, and K. Foreste, 2012, 4D close-the-loop using probabilistic seismic inversion on the Astokh field, offshore Sakhalin: 74th European Association of Geoscientists and Engineers Conference and Exhibition: Responsibly Securing Natural Resources, 648–652.
- Kohonen, T., 1982, Self-organized formation of topologically correct feature maps: *Biological Cybernetics*, **43**, 59–69, doi: [10.1007/BF00337288](https://doi.org/10.1007/BF00337288).
- Li, F., and W. Lu, 2014, Coherence attribute at different spectral scales: *Interpretation*, **2**, no. 1, SA99–SA106, doi: [10.1190/INT-2013-0089.1](https://doi.org/10.1190/INT-2013-0089.1).
- MacBeth, C., M. Floricich, and J. Soldo, 2006, Going quantitative with 4D seismic analysis: *Geophysical Prospecting*, **54**, 303–317, doi: [10.1111/j.1365-2478.2006.00536.x](https://doi.org/10.1111/j.1365-2478.2006.00536.x).
- MacBeth, C., Y. HajNasser, K. Stephen, and A. Gardiner, 2011, Exploring the effect of meso-scale shale beds on a reservoir's overall stress sensitivity to seismic waves: *Geophysical Prospecting*, **59**, no. 1, 90–110.
- Marfurt, K. J., 2018, Seismic attributes as the framework for data integration throughout the oilfield life cycle: SEG.
- Matos, M., P. Osorio, and P. Johann, 2006, Unsupervised seismic facies analysis using continues wavelet transform and self-organizing maps: *Geophysics*, **72**, no. 1, P9–P21, doi: [10.1190/1.2392789](https://doi.org/10.1190/1.2392789).
- McConnell, H., and N. Pannell, 2018, Maui 4D seismic survey: Marine mammal impact assessment: SLR Consulting NZ limited.
- Murray, D., 2010, Maui-5 A well completion report: NZP&M, Ministry of Business, Innovation & Employment (MBIE), New Zealand Unpublished Petroleum Report PR4275.
- Murray, D., D. Hadley, J. Davies, and I. Mostafa, 2010, MB-03A, MB-05B, and MB-11A/B well completion report: NZP&M, Ministry of Business, Innovation & Employment (MBIE), New Zealand Unpublished Petroleum Report PR4275.
- Naeini, E. Z., H. Hoeber, G. Poole, and H. R. Siahkoohi, 2009, Simultaneous multivintage time-shift estimation: *Geophysics*, **74**, no. 5, V109–V121, doi: [10.1190/1.3177002](https://doi.org/10.1190/1.3177002).
- Nasser, M., C. Gronister, B. Hay, and C. Amos, 2017, 4D seismic close-the-loop impacts business decisions at the Okume complex, Equatorial Guinea: The Leading Edge, **36**, 394–400, doi: [10.1190/tle36050394.1](https://doi.org/10.1190/tle36050394.1).
- Pannett, S., S. Slager, G. Stone, and S. Dekker, 2004, Constraining a complex gas-water dynamic model using 4D seismic: Presented at the Annual Technical Conference and Exhibition, 209–225, SPE.
- Partyka, G., J. Gridley, and J. Lopez, 1999, Interpretational applications of spectral decomposition in reservoir characterization: The Leading Edge, **18**, 353–360, doi: [10.1190/1.1438295](https://doi.org/10.1190/1.1438295).
- Rangel, R., C. Macbeth, and M. Mangriots, 2016, The effect of shale activation on 4D seismic interpretation of a UKCS field: Presented at the 78th Conference and Exhibition, EAGE.
- Roden, R., T. Smith, and D. Sacrey, 2015, Geologic pattern recognition from seismic attributes: Principal component analysis and self-organizing maps: *Interpretation*, **3**, no. 4, SAE59–SAE83, doi: [10.1190/INT-2015-0037.1](https://doi.org/10.1190/INT-2015-0037.1).
- Roden, R., T. Smith, P. Santogrossi, D. Sacrey, and G. Jones, 2017, Seismic interpretation below tuning with multiattribute analysis: The Leading Edge, **36**, 330–339, doi: [10.1190/tle36040330.1](https://doi.org/10.1190/tle36040330.1).
- Rojas, N., and T. L. Davis, 2009, Spectral decomposition applied to time-lapse seismic interpretation, Rulison

- Field, Colorado: 79th Annual International Meeting, SEG, Expanded Abstracts, 3845–3849, doi: [10.1190/1.3255669](https://doi.org/10.1190/1.3255669).
- Roy, A., M. M. C. De Matos, and K. J. Marfurt, 2011, Application of 3D clustering analysis for deep marine seismic facies classification — An example from deep-water northern Gulf of Mexico: Gulf Coast Section SEPM 31st Annual Bob. F. Perkins Research Conference, 410–439.
- Roy, A., B. L. Dowell, and K. J. Marfurt, 2013, Characterizing a Mississippian Tripolitic Chert reservoir using 3D unsupervised seismic facies analysis and well logs: An example from Osage County, Oklahoma: Interpretation, **1**, no. 2, SB109–SB124, doi: [10.1190/INT-2013-0023.1](https://doi.org/10.1190/INT-2013-0023.1).
- Russell, B. H., 1988, Introduction to seismic inversion methods: SEG.
- Sengupta, M., G. Mavko, and T. Mukerji, 2003, Quantifying subresolution saturation scales from time-lapse seismic data: A reservoir monitoring case study: Geophysics, **68**, 803–814, doi: [10.1190/1.1581033](https://doi.org/10.1190/1.1581033).
- Strecker, U., and R. Uden, 2002, Data mining of 3D post-stack seismic attribute volumes using Kohonen self-organizing maps: The Leading Edge, **21**, 1032–1037, doi: [10.1190/1.1518442](https://doi.org/10.1190/1.1518442).
- Taner, M. T., 2001, Seismic attributes: Canadian Society of Exploration Geophysicists Recorder, **26**, 1–15.
- Telford, C., and D. Murray, 2008, MA-02A well completion report: NZP&M, Ministry of Business, Innovation & Employment (MBIE), New Zealand Unpublished Petroleum Report PR4275.
- Thangam, A., 2013, MA-04A well completion report: NZP&M, Ministry of Business, Innovation & Employment (MBIE), New Zealand Unpublished Petroleum Report PR4821.
- Thangam, A., 2015, MA-09A and MA-09B well completion report: NZP&M, Ministry of Business, Innovation & Employment (MBIE), New Zealand Unpublished Petroleum Report PR4821.
- Tian, S., A. Shams, and C. MacBeth, 2014, Closing the loops using engineering-consistent 4D seismic inversion: The Leading Edge, **33**, 188–196, doi: [10.1190/tle3302018.1](https://doi.org/10.1190/tle3302018.1).
- Van der Veeken, 2016, 4D PreSDM processing for the Maui base and monitor surveys: NZP&M, Ministry of Business, Innovation & Employment (MBIE), New Zealand Unpublished Petroleum Report, PR5377.
- White, J. C., G. A. Williams, S. Grude, and R. A. Chadwick, 2015, Utilizing spectral decomposition to determine the distribution of injected CO₂ at the Snøhvit Field: Geophysical Prospecting, **63**, 1213–1223, doi: [10.1111/1365-2478.12217](https://doi.org/10.1111/1365-2478.12217).
- Xue, Y., 2013, Novel stochastic inversion methods and workflow for reservoir characterization and monitoring: Ph.D. dissertation, The University of Texas at Austin.
- Zhao, B., D. H. Johnston, and W. Gouveia, 2006, Spectral decomposition of 4D seismic data: 76th Annual International Meeting, SEG, Expanded Abstracts, 3235–3239, doi: [10.1190/1.2370202](https://doi.org/10.1190/1.2370202).
- Zhao, T., J. Zhang, F. Li, and K. J. Marfurt, 2016, Characterizing a turbidite system in Canterbury Basin, New Zealand, using seismic attributes and distance-preserving self-organizing maps: Interpretation, **4**, no. 1, SB79–SB89, doi: [10.1190/INT-2015-0094.1](https://doi.org/10.1190/INT-2015-0094.1).



Marwa Hussein received a B.S. (2010) and an M.S. (2014) in geophysics from Ain Shams University, Cairo. She later received a Ph.D. in geophysics from the University of Houston, USA. Her research interests include advanced seismic interpretation techniques, seismic attribute analysis, reservoir characterization, machine learning, and time-lapse seismic studies.



Robert R. Stewart received a B.S. in math and physics from the University of Toronto and a Ph.D. in geophysics from the Massachusetts Institute of Technology. He was employed with Chevron's Oil Field Research Lab, California, ARCO in Dallas, and Veritas Software, Calgary. He was professor of geophysics at the University of Calgary, held its chair in exploration geophysics, and co-founded the CREWES Project, a university-industry consortium. In 2008, he joined the University of Houston (UH) as professor of geophysics, holds the Cullen Chair in Exploration Geophysics, and is director of the Allied Geophysical Laboratories. He received UH's Natural Sciences and Mathematics Teaching Excellence Award in 2013, the UH Provost's Teaching Excellence Award in 2014, and the 2019 Team Teaching Award. He is a licensed geoscientist in Alberta and Texas. He has published more than 180 papers in geoscience journals and magazines and holds two patents. He was the SEG Distinguished Educator and received the SEG Lifetime Membership Award. He also served as president of the Canadian SEG and received its Honorary Membership Award and Medal. He completed service as the first vice president of the Geophysical Society of Houston and is a past president of SEG.



Deborah Sacrey received her degree (1976) in geology from the University of Oklahoma and immediately started working for Gulf Oil in their Oklahoma City offices. She is a geologist/geophysicist with 43 years of oil and gas exploration experience in the Texas and Louisiana Gulf Coast and Mid-Continent areas of the United States. She started her own company, Auburn Energy, in 1990 and built her first geophysical workstation using Kingdom software in 1996. She helped SMT/IHS for 18 years in developing and testing the Kingdom Software. She specializes in 2D and 3D interpretation for clients in the United States and internationally. For the past nine

years, she has been part of a team to study and bring the power of multiattribute neural analysis of seismic data to the geoscience public, guided by Tom Smith, founder of SMT. She has become an expert in the use of Paradise software and has seven discoveries for clients using multiattribute neural analysis. She has been very active in the geologic community. She is past national president of the Society of Independent Professional Earth Scientists (SIPES), past president of the Division of Professional Affairs of AAPG, past treasurer of AAPG, and past president of the Houston Geological Society. She is also past president of the Gulf Coast Association of Geological Societies and is one of the GCAGS representatives on the AAPG Advisory Council. She is also a DPA Certified Petroleum Geologist 4014 and DPA Certified Petroleum Geophysicist 2. She is a member of AAPG, SIPES, the Houston Geological Society, the South Texas Geological Society, and the Oklahoma City Geological Society.



David H. Johnston received a B.S. (1973) in earth sciences from the Massachusetts Institute of Technology (MIT) and a Ph.D. (1978) in geophysics, also from MIT. He is the managing director of Differential Seismic, LLC, a geophysics consultancy. He retired from ExxonMobil in 2017 after a 38-year career in research, exploration,

and production. He was responsible for the development and commercialization of 4D seismic technology in Exxon-Mobil, and he was geophysics coordinator for ExxonMobil Production Company where he provided technical and business stewardship of ExxonMobil's global production geophysics activity. He is a licensed geoscientist (PG) in Texas. He has more than 75 publications and professional society presentations. He was an editor of *Seismic wave attenuation* (1981), *Reservoir geophysics* (1992), and *Methods and applications in reservoir geophysics* (2010), all published by SEG. He is also the author of *Practical applications of time-lapse seismic data* (2013). He has received several awards from SEG including life membership, and in 2013 he served as the SEG Distinguished Short Course Instructor.



Jonny Wu received a B.E. (1998) in geologic engineering from the University of Waterloo, Canada, and worked for Shell Canada for five years as an exploration geologist. He then received an M.S. (2006) and a Ph.D. (2010) in geology from Royal Holloway, University of London, UK, followed by a postdoctoral fellowship at National Taiwan University, Taiwan. His current research interests include plate tectonic reconstructions, structural geology and fault dynamics, and Asia tectonics.